

## In situ analysis of capturing dynamics of magnetic nanoparticles in a microfluidic system

Ahsan Munir<sup>1</sup>, Zanzan Zhu<sup>1</sup>, Jianlong Wang<sup>2</sup> and H. Susan Zhou<sup>\*1</sup>

<sup>1</sup>Department of Chemical Engineering, Worcester Polytechnic Institute, 100 Institute Road, Worcester, Massachusetts 01609, USA

<sup>2</sup>College of Food Science & Engineering, Northwest A&F University, 28 Xinong Road, Yangling, Shaanxi 712100, China

(Received June 11, 2012, Revised November 10, 2012, Accepted November 30, 2012)

**Abstract.** Magnetic nanoparticle based bioseparation in microfluidics is a multiphysics phenomenon that involves interplay of various parameters. The ability to understand the dynamics of these parameters is a prerequisite for designing and developing more efficient magnetic cell/bio-particle separation systems. Therefore, in this work proof-of-concept experiments are combined with advanced numerical simulation to design and optimize the capturing process of magnetic nanoparticles responsible for efficient microfluidic bioseparation. A low cost generic microfluidic platform was developed using a novel micromolding method that can be done without a clean room techniques and at much lower cost and time. Parametric analysis using both experiments and theoretical predictions were performed. It was found that flow rate and magnetic field strength greatly influence the transport of magnetic nanoparticles in the microchannel and control the capturing efficiency. The results from mathematical model agree very well with experiments. The model further demonstrated that a 12% increase in capturing efficiency can be achieved by introducing of iron-grooved bar in the microfluidic setup that resulted in increase in magnetic field gradient. The numerical simulations were helpful in testing and optimizing key design parameters. Overall, this work demonstrated that a simple low cost experimental proof-of-concept setup can be synchronized with advanced numerical simulation not only to enhance the functional performance of magneto-fluidic capturing systems but also to efficiently design and develop microfluidic bioseparation systems for biomedical applications.

**Keywords:** microfluidics; magnetic nanoparticles; bioseparation; lab-on-a-chip; mathematical modelin

### 1. Introduction

Magnetic field-assisted separation of biomolecules in microfluidic systems has received increased attention in the last decade due to its vast applications in biomedical engineering research, clinical diagnostic and biotechnological sciences. The idea behind this innovative technology involves isolating biomolecules of interest from the bulk mixture by attaching them to magnetic particles and then recovering it using an external magnetic field (Manz *et al.* 1990, Pamme 1996, Ahn *et al.* 1996, Pankhurst *et al.* 2003, Deng *et al.* 2002, Berry and Curtis 2003). In the past few years, several microfluidic system incorporating magnetic-actuation have been

---

\*Corresponding author, Professor, E-mail: [szhou@wpi.edu](mailto:szhou@wpi.edu)

successfully developed for separation and detection of biomolecules (Choi *et al.* 2002, Bu *et al.* 2008), immunoassay of proteins (Hahn *et al.* 2007, Hayes *et al.* 2001), purification of DNA (Lehmann *et al.* 2006), and cell separation (Xia *et al.* 2006). Most of these system are based on functionalized magnetic beads or microparticles (Pamme 2006, Xia *et al.* 2006, Bu *et al.* 2008, Smistrup *et al.* 2006), however there are relative few microfluidic systems (Shih *et al.* 2008) in literature that have employed magnetic nanoparticles (MNPs) for separation of biomolecules. Compared with microparticles, MNPs possess better properties that can advantageously be used in microfluidic devices, such as their extremely small size causes minimal disturbance to attached biomolecules (Gijs 2004). MNPs also possesses higher surface to volume ratio (Gijs 2004) that can bring out efficient chemical binding and most importantly they are super-paramagnetic (Gijs 2004), i.e., their magnetization without a magnetic field is zero. The super-paramagnetic nature ensures that they stay suspended in carrier liquid when the magnetic field is removed without giving agglomeration issues as can be seen in microparticles or microbeads. This makes it easy for the removal or capture of tagged biomolecules of interest and better interaction with biomolecules like cells, proteins, DNA etc. McCloskey *et al.* (2001) showed that the number of binding sites for MNPs increases with decrease in the size of MNPs. This translates into higher magnetic force acting on cells which eventually will give higher separation efficiencies. Overall, inclusion of magnetic nanoparticles in microfluidic devices will greatly enhance the device functionality and separation performance.

The separation of biomolecules not only depends on the use of magnetic nanoparticles but is also a multiphysics phenomenon that involves interplay of various other parameters such as inlet velocity, MNP size, magnetic field strength and its orientation, geometry of the device etc. In order to design and develop more robust magnetic microfluidic system it is important to understand how these parameters influence each other. Proof of concept experiments together with mathematical modeling can reveal the dynamics of this process and will be very helpful in designing, optimizing and developing more efficient magnetic microfluidic bioseparation system. To date several groups have reported (Kim *et al.* 2006, Furlani *et al.* 2001, Furlani 2006, Furlani and Ng 2006, McCloskey *et al.* 2000, Brauer *et al.* 2007, Clime *et al.* 2007) the study of the transport of magnetic particles in microfluidic system but most of these were focused on microparticles or microbeads. Moreover, only simple magnetic field configurations were considered without a detailed analysis and optimization strategies. Recent advances in MEMS technology has helped researcher to develop systems for manipulation of microparticles (Lee *et al.* 2001). Experimental investigations have so far focused on qualitative demonstrations of capture (Smistrup *et al.* 2005, Rida and Gijs 2004) or separation (Yellen and Friedman 2004) using microfabricated electromagnets. While useful, these investigations lack detailed quantitative analysis that can be used for designing more simple and robust systems. Moreover, these devices require expensive fabrication processes or clean room techniques in order to integrate the magnets with the microfluidic channels to achieve magnetic particles capturing and separation. A microfluidic system that allows a simple fabrication procedure while achieving the same functional purpose of magnetic based separation is also highly desirable.

In this work, a simple, low cost and generic microfluidic platform is assembled to study the dynamics of magnetic nanoparticle capturing process. Standard molding process combined with a novel rapid prototyping method is used to develop low cost polydimethylsiloxane (PDMS) microchannel. The fabrication method used in this work circumvents the requirement for a clean room. It also eliminates the combination of two pieces of element, such as in standard fabrication method where negative or positive stamp on PDMS are combined with glass or silicon using

plasma as a result overcomes the problem of leakage. Magnetic nanoparticle dynamics in microchannel is studied using an experimental setup containing a sub-microliter fluid volume surrounded permanent magnet systems for particle capturing. On the basis of MNPs concentration measurement using optical technique, capturing efficiency analysis is performed. Influence of flow rate conditions, magnetic field systems on the capturing efficiency is investigated. A finite-element-based mathematical model is also developed to predict the dynamics of the magnetic nanoparticle loaded fluid. The simulations are found to be in good agreement with the experimental results. Parametric investigations using both experiments and theoretical predictions illustrate the effects of flow and magnetic parameters on the MNPs capturing efficiency in the microchannel and agree very well with each other. Mathematical model is further used to enhance the performance of the proof-of-concept study performed using the experimental setup. A novel idea of incorporating a grooved iron bar in close proximity to a microfluidic channel is tested using the numerical simulation. The presence of external grooved shape iron bar altered the magnitude of the magnetic field density gradient inside the microchannel. This results in an increase in capturing efficiency due to higher magnetic force acting on the MNPs. This work demonstrates that a simple low cost experimental proof-of-concept setup can be synchronized with advanced numerical simulation to design and improve the functional performance of magneto-fluidic bioseparation systems based on magnetic nanoparticles.

## **2. Experimental materials and methods**

### *2.1 Microchannel fabrication*

The microfluidic channels with a diameter of 500  $\mu\text{m}$  and length of 75 mm were fabricated by a low cost rapid micromolding technique. First, a mold was prepared by fixing an aluminum wire of 500  $\mu\text{m}$  diameter in the center and approximately at half the depth of the empty Petri dish. Polydimethylsiloxane (PDMS)(Sylgard 184, Dow Corning, USA) with a base and curing agent mixed in a ratio of 10:1 was poured onto the mold and was degassed to remove any bubbles using desiccators. The uncured PDMS was baked in an oven (65°C) for 1 h. The final step was to peel off the cured-PDMS containing the aluminium wire from the Petri dish. The sides of the cured PDMS were cut using a razor blade, leaving a significant amount of the wire exposed outside. With the help of pliers the wire were carefully removed. To make this process easier, the microchannel were washed with acetone which swelled the PDMS and expanded the channels prior to pulling out the wires. The microchannel was connected with the tygon tubing using the stainless tip obtained from microsyringe. The tip was inserted into the microchannel to make leakage free connection.

### *2.2 Microfluidic system setup*

A schematic view together with experimental set-up to carry out magnetic nanoparticle capturing in microfluidic channel is shown in Figs. 1(a) and 1(b). The magnetic and microfluidic set-up may be divided in five main components: the microchannel, the magnetic nanoparticles solution, the fluidic connections, the imaging instrumentation, and the permanent magnet system. As shown in Fig. 1, the microfluidic channel is connected with inlet and outlet via flexible tygon tubing. In order to provide leak free connections a microsyringe tips made of stainless steel are

embedded into the microchannel inlet/outlet for secure connections between the flexible tubes and the microfluidic chip. A differential pressure drop is maintained inside the channel by connecting the outlet of the microchannel to peristaltic micropump (P625 Peristaltic Pump, Instech, USA) and inlet to reservoir containing MNPs solution. Flow rate were varied using the precise-bi directional speed controller on the pump. This simple method allows for a good control of the flow in the channel in suction mode. Magnetic field is provided by assembly of permanent neodymium magnets (KJ Magnetics, USA). Magnetic system assembly comprising of different shapes and strength of neodymium magnets as illustrated in Table 1, were used in the vicinity of the microchannel. The approximate strength of magnetic assemblies was calculated based on the finite element simulation described later in the section. Optical images in the region of interest (ROI) (see Fig. 1(c)) were acquired using the digital microscope (Celestron 44340, Celestron Inc., USA). The translational stage of the microscope was used to place the microfluidic chip assembly such that the objective of camera acquires images of the flowing nanoparticles both in static and in real time. The CCD camera was connected to a computer for data acquisition. Image acquisition was performed using ImageJ software (NIH, USA) from the region of interest (ROI) under bright field lightning condition.

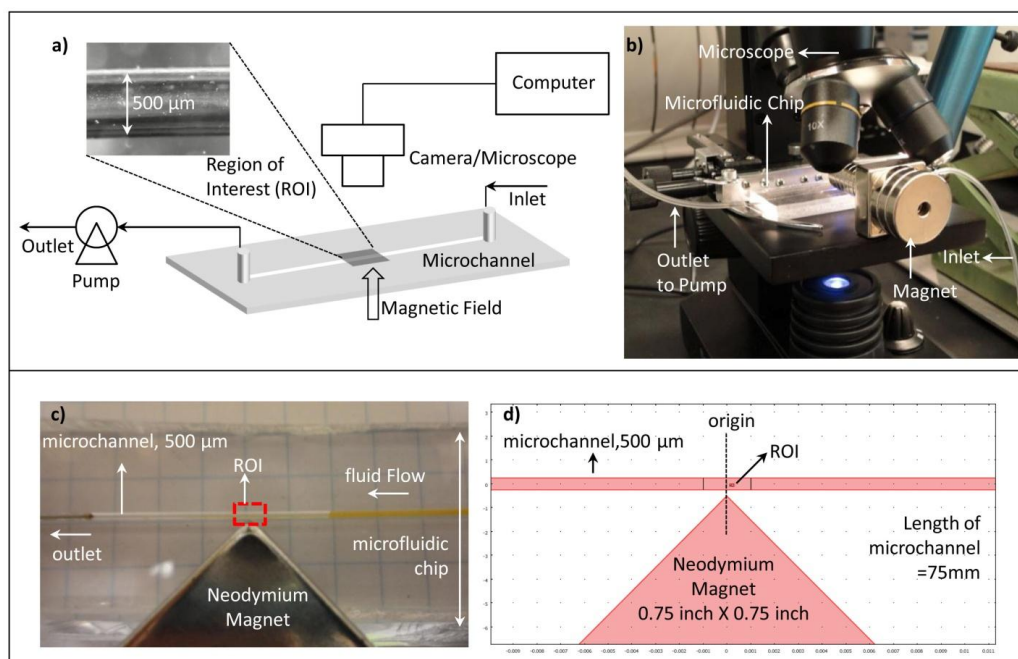


Fig. 1 Microfluidic Magnetic Nanoparticle Capturing System; (a) schematic of the experimental setup, (b) snapshot of the setup showing microfluidic platform with inlet and outlet connections through tubings, permanent magnet in the vicinity of microfluidic chip, and the objective of microscope over the region of interest (ROI) for recording images. Inset shows the size of ROI and microchannel diameter, (c) experimental setup showing ROI within the microchannel with neodymium magnet placed at its edge (System 8), and (d) Finite Element Model setup in COMSOL for simulating the scenario given in (c). (Length of channel=75 mm)

Table 1 Specification of Magnetic System Assembly used in Capturing MNPs

System	Specification (Inch)				Effective width <sup>a</sup>	Length	Magnetic Flux density
	Square (0.75 × 0.75)	Circular (D=0.75)	Circular (D=0.50)	Rectangle (0.75 × 0.375)	Inch	Inch	Tesla (T)
1	0	14	0	0	0.75	1.75	0.236
2	1	14	0	0	0.75	2.5	0.276
3	0	0	22	0	0.5	1.375	0.229
4	0	0	0	20	0.375	1.25	0.138
5	1	0	0	20	0.375	1.5	0.177
6	1	14	0	20	0.75	3.25	0.264
7	1 (Flat)	0	0	0	0.75	0.75	0.45 <sup>b</sup>
8	1 (Edge)	0	0	0	0.75	0.75	0.645 <sup>b</sup>

<sup>a</sup> Surface width of magnet close to the wall of microchannel

<sup>b</sup> Magnet system is close to the wall of microchannel

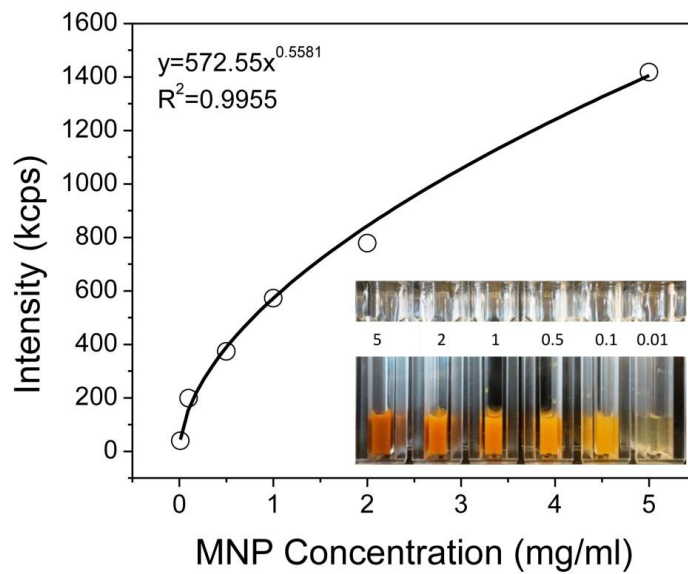


Fig. 2 Calibration Curve obtained for MNPs using scattering intensity obtained from Zetasizer Nano S. Inset shows different concentrations of MNPs used in generating calibration curve

Magnetic nanoparticles (MNPs) of 200 nm diameter (fluidMAG-ARA Chemicell GMBH, Germany) were suspended in de-ionized DI water and injected into the inlet. The magnetic nanoparticles consisted of an inner core made up of magnetite (Fe<sub>3</sub>O<sub>4</sub>) crystals of approximately 12 nm diameter, embedded in a biocompatible polysaccharide matrix for better stability that also prevented biodegradation. The overall diameter of the nanoparticles was approximately 200 nm, whereas the volume fraction of magnetite within a composite particle is 20%. For different flow rates, effluent was collected at the outlets once all the solution has passed through the

microchannel. The volume collected at the outlet was regularly verified to confirm the equal flow rates in the microchannel. The concentration of MNPs solution in the effluent was estimated from in-house determined calibration curve. The calibration curves were generated from original stock of MNPs solution diluted to different concentrations. A dynamic light scattering instrument (Malvern Zetasizer Nano S, UK) was used. The Zetasizer Nano S measures the intensity of scattered light of various concentrations of sample at one angle; this is compared with the scattering produced from a standard (i.e., Toluene). In general, Zetasizer is used to measure the size of molecules but also the count rate can be used as a method of determining the relative concentration of a sample of stable size—as the count rate goes down, so does the concentration. While the Zetasizer software does not automatically produce an estimated sample concentration from the count rate, it is actually a fairly stable value for the same sample over time, and therefore is used in this work as an estimate of concentration. Power law calibration curve of scattering intensity (kilocounts per second, kcps) versus concentration of magnetic nanoparticles (mg/ml) were obtained for 200 nm particles ( $R^2=0.9908$ ) (see Fig. 2). In order to obtain capturing efficiency ( $CE_{\text{experiment}}$ ) of the system under various condition of magnetic field strength and flow rate, the outlet sample from the effluent was taken in cuvette and placed in Zetsizer to obtain unknown scattering intensity (kcps) of the sample. Calibration curve was used to convert the scattering intensity into concentration (mg/ml). Since the inlet concentration of MNPs was known, capturing efficiency was calculated by subtracting the ratio of outlet to inlet concentration from 1.

### 3. Model development

A finite element mathematical model was implemented keeping the following objective in mind; i) to investigate the interaction of external magnetic field with the flow of magnetic nanoparticles, ii) to predict and validate the experimental proof-of-concept study, and iii) to implement a novel idea in the system for enhancing the performance. The two-dimensional geometrical representation of a microfluidic channel with a permanent magnet as used in experiments is shown in Fig. 1(d). It was assumed that the mass transport variation under the influence of magnetic field will be negligible in the direction perpendicular to the x-y plane due to high aspect ratio (Sullivan *et al.* 2007) of the system modeled. This will reduce the 3D geometry to a 2D thereby significantly decreasing the computational overhead. Moreover, a 2D model will serve as a simple, fast, and relatively accurate guideline for designing and optimizing magnetic microfluidic systems for bioseparation.

The 2D model geometry as shown in Fig. 1(d) consists of a microchannel which is 500  $\mu\text{m}$  wide and 75 mm long. A magnetic field assembly comprising of a 0.75 x 0.75 inch square neodymium magnet is placed closed to the microchannel with one of its edge very close to the microchannel. This geometry is chosen to represent the system 8 (see Table 1) magnetic field assembly. The magnetic nanoparticles are assumed to be dispersed in the water and flow from right to left. The transport of a magnetic nanoparticle in a carrier fluid (eg: water) is governed by the following major factors including (a) the magnetic force, arising from magnetic field and strong magnetic field gradient created from external permanent magnet, (b) the viscous drag, due to movement of magnetic nanoparticles with respect the surrounding fluid, (c) fluid-particle interactions, due to perturbations produced in the flow field, (d) gravity/buoyancy, (e) thermal kinetics (Brownian motion), and (h) inter-particle effects. In the experimentation a low concentration of MNPs was used therefore particle/fluid interactions and inter-particle effects were

neglected in the analysis. Moreover, the size of MNPs was extremely small (~200 nm) therefore gravity effects were neglected but Brownian motion (Furlani 2010, Gerber *et al.* 1983) was included by incorporating a drift-diffusion equation for simulating the behavior of a concentration of magnetic nanoparticles. The equations and theory developed are based on Navier-Stokes equations for solving flow field of carrier fluid (in this case it is assumed water), drift diffusion equation for mass transport of MNPs, and Maxwell's equations to predict magnetic field and magnetic force in the microchannel. The model basically solves the Maxwell's equation for a static magnetic field. The computed magnetic force is coupled to fluid flow by using the magnetic volume force term acting on the nanoparticles in the Navier-Stokes equations, which accounts for the momentum transfer from the MNPs to the fluid (particle-fluid interaction). A drift-diffusion equation was used to predict the nanoparticle concentration which was dependent on flux contributions from diffusion, advection, and magnetic force-based migration. The detailed explanation of the equations and theory used in the model are described in the following sections.

### 3.1 Magneto-static equations

The static magnetic field is calculated using Maxwell-Ampere's law given by

$$\nabla \times H = J \quad (1)$$

Where  $H$  is the magnetic field vector ( $A/m$ ) and  $J$  is the current density vector ( $A/m^2$ ), According to Gauss law for magnetic flux density,  $B$  ( $Vs/m^2$ )

$$\nabla \cdot B = 0 \quad (2)$$

In order to describe a relation between  $B$  and  $H$ , a constitutive relation given by the following equation is used for permanent magnet in the model.

$$B = \mu H + B_R \quad (3)$$

Where,  $\mu$  is the magnetic permeability which can also be expressed as  $\mu_0 \mu_r$  where  $\mu_r$  is the relative permeability of magnet ( $\mu_r = 1$ ) and is assumed to be constant in all the simulations and  $\mu_0$  is the permeability in vacuum ( $\mu_0 = 4\pi \times 10^{-7} N/A^2$ ).  $B_R$  is the remanent flux density and for Neodymium Magnet used in the simulation it assigned as 1.3T. The magnetic permeability A magnetic vector potential  $A$  is described (Rosensweig 1997) according to the following equation

$$\nabla \times A = B; \nabla \cdot A = 0 \quad (4)$$

After substitution of equation 4 in Eqs. (1), (2) and (3), the following vector equation is obtained

$$\nabla \times \left( \frac{1}{\mu_0 \mu_r} \nabla \times A - M \right) = J \quad (5)$$

It is assumed that the magnetic vector potential has a nonzero component only perpendicular to the plane  $A_z$  which basically simplifies the 2D and it has perpendicular current equals to zero. Based on these assumption Eq. (5) simplifies to following equation

$$\nabla \times \left( \frac{1}{\mu_0 \mu_r} \nabla \times A - M \right) = 0 \quad (6)$$

Given the magnetic field,  $H$  obtained using Eq. (6), magnetic force that is exerted on the magnetic nanoparticles is calculated using the following equation Suzuki *et al.* (2004)

$$F_m = (1 - N_d) \mu_0 \mu_r \alpha V_{MNP} (H \cdot \nabla) H \quad (7)$$

Where,  $N_d$  is the demagnetizing factor (0.33 for a sphere),  $V_{MNP}$  is the volume of a magnetic nanoparticles, and  $\alpha$  is the ratio of iron oxide content which is 0.8 for the magnetic nanoparticles used in this work.

#### Boundary Conditions

A magnetic insulation boundary condition ( $A_z = 0$ ) was applied along the system boundary.

### 3.2 Fluid flow equation

The magnetic nanoparticles (MNPs) were assumed to be dispersed in the fluid of viscosity  $\eta$  ( $10^{-3} \text{ kg/m}\cdot\text{s}$ ) and density  $\rho$  ( $10^3 \text{ kg/m}^3$ ) equal to that of water. The aqueous solution of MNPs is injected into the microchannel with a parabolic velocity. The magnetic force acting on MNPs due to external magnetic field transfers momentum to the surrounding fluid leading to a disturbance in flow profile of carrier liquid. The flow velocity  $u$  for this incompressible fluid ( $\nabla \cdot u = 0$ ) is described using Navier-Stokes equation

$$\rho \frac{\partial u}{\partial t} + \rho (u \cdot \nabla) u = -\nabla p + \eta \nabla^2 u + F_{Vol} \quad (8)$$

Where,  $u$  is the carrier fluid velocity field ( $m/s$ ),  $p$  is the pressure ( $N/m^2$ ), and  $F_{Vol}$  is the volume force ( $N/m^3$ ). The momentum transfer from MNPs to the fluid is incorporated by setting the volume force term equal to the magnetic force acting on a single MNP multiplied with MNP number density,  $\chi$ , which is the number of MNP per unit volume. Therefore, the volume force acting on fluid is given by

$$F_{Vol} = \chi F_m \quad (9)$$

Eq. (9) couples the fluid flow equation with the magnetic field equation and depends on the instantaneous concentration of MNP solution in the microchannel, which is described in more detail later section. MNP number density ( $\chi$ ) is calculated using Eq. (10).

$$\chi = \frac{6CM_{Fe_3O_4} \times 10^{-3}}{\rho_m \pi d_p^3} \quad (10)$$

Where,  $C$  is the concentration of MNPs ( $\mu M$ ),  $M_{Fe_3O_4}$  is the molar mass of  $Fe_3O_4$  ( $g/mol$ ),  $\rho_m$  is the density of MNPs ( $g/cm^3$ ), and  $d_p$  is the diameter of MNPs ( $cm$ ). It is also assumed that there is no particle-particle interaction (e.g., Van der Waals forces) and even the sedimentation effects will have negligible influence on the overall mass transport due to extremely small size of MNPs.

#### Boundary Conditions

The flow of fluid at the inlet is assumed to be parabolic and moves in the direction of x-axis with zero velocity in y-direction. The average flow velocity of carrier fluid is  $u_0$ . No slip condition ( $u = v = 0$ ) is applied along the walls of microfluidic system and at the outlet, pressure condition is set equal to zero.

#### *3.3 Drift-diffusion equation*

The spatial and temporal variation of the MNP solution inside the microfluidic channel is described using the drift-diffusion equation where Brownian motion due to extremely small size of nanoparticle was also taken into account Gerber (1983) Specifically,  $C$  the concentration of MNP solution is governed by the following equation (Furlani 2006, Furlani and Ng 2006, McCloskey *et al.* 2000)

$$\frac{\partial C}{\partial t} + \nabla \cdot J = 0 \quad (11)$$

Where  $J = J_D + J_A$  is the total flux of nanoparticles, which includes a contribution from diffusion,  $J_D = -D\nabla C$ , and a contribution  $J_A = u_p C$ , due to the advection of the nanoparticles under the influence of applied forces. The drift velocity  $u_p$  of MNPs is obtained using classical Newtonian particle motion equation (Furlani 2006) as described below.

$$m_p \frac{\partial u_p}{\partial t} = F_m + F_g + F_D \quad (12)$$

In the limit of negligible inertia ( $m_p \frac{\partial u_p}{\partial t} \rightarrow 0$ ) and zero gravitational force,  $F_g$ , Eq. (12) results in Eq. (13)

$$F_m + F_D = 0 \quad (13)$$

Where  $F_m$  and  $F_D$  are magnetic and drag forces respectively. According to Stokes' law of

viscous drag,  $F_D = -6\pi\eta r_p(u_p - u)$ , where  $u_p$  and  $r_p$  is the MNPs velocity and radius respectively,  $u$  is the fluid velocity of viscosity  $\eta$  ( $10^{-3} \text{ kg/m}\cdot\text{s}$ ). Therefore, from Eq. (13)

$$F_m - 6\pi\eta r_p(u_p - u) = 0 \quad (14)$$

Since the mobility of the particle is given by  $\gamma = 1/6\pi\eta r_p$  Eq. (14) can be re-written as

$$u_p = u + \gamma F_m \quad (15)$$

Substituting Eq. (15) in flux,  $J_A$  Eq. (11) can be re-written as

$$\frac{\partial C}{\partial t} = D\nabla^2 C - u\nabla C - (\gamma F_m)\nabla C \quad (16)$$

Where diffusion coefficient  $D$  is calculated using Nernst-Einstein relation  $D = \gamma kT$

#### Boundary Conditions

An initial unmixed concentration of MNP solution is injected into the microchannel on the right boundary. Convective flux is set at the outlet boundary on the left, keeping insulation/symmetry in all the other boundaries.

### 3.4 Numerical simulation

A finite element software package, COMSOL™ was used to solve the partial differential equations described above in the model. The model consisted of one geometry and three application modes including magnetostatics to obtain static magnetic field produced by the permanent magnet, incompressible Navier-Stokes to predict velocity profile of carrier fluid, and convection diffusion to simulate spatial and temporal variation of the MNP solution inside the microfluidic channel. The meshing around the geometry was around 10  $\mu\text{m}$  except for the channel inlet and outlet where more fine elements (1  $\mu\text{m}$ ) were used in order to resolve the domain. The model was solved in two steps using two different solvers. First the magnetic field and magnetic forces generated due to permanent magnetic was solved using the magnetostatic application mode with a non-linear solver and then a time-dependent solver was used to solve incompressible Navier-Stokes application mode together with convection diffusion equation.

### 3.5 Capturing Efficiency ( $CE_{\text{numerical}}$ )

Magnetic nanoparticle concentration rate (mg/s) at the inlet and outlet of the microchannel was computed using the total normal flux (mg/m.s) multiplied by the cross-section length of the channel at the inlet and outlet. In order to obtain the incoming ( $M_{in}$ ) and outgoing mass ( $M_{out}$ ) of magnetic nanoparticles, a numerical integration method (trapezoidal rule) was used to approximate the integral or the area under a curve of magnetic nanoparticle concentration rate (mg/s) versus time. Capturing efficiency was later obtained using the following equation

$$CE_{numerical} = \left( 1 - \frac{M_{out}}{M_{in}} \right) \times 100 \tag{17}$$

## 4. Results and discussion

### 4.1 Magnetic field measurements

Prior to more detailed parametric investigation, magnetic field strength for different permanent magnet assembly (see Table 1) was computed using the numerical model described for magneto-static equation in section 3.1. The magnetic flux density calculations were also validated using the well developed analytical expressions given by Furlani *et al.* The numerical results agree very well with the analytical solution and the range of magnetic flux density (0.12-0.2 Tesla) computed using the numerical model for different magnetic system assembly was also almost of same order of magnitude as reported in real microfluidic devices (Bu *et al.* 2008, Gijss 2004).

Computed Magnetic flux density at the center of microchannel along the x-axis for different magnetic system assemblies are given Fig. 3. It can be seen that system 2 and system 6 produced maximum magnetic field with system 4 producing the least amount inside the microchannel. The magnetic field strength is dependent on shape, size, and grade of neodymium magnets used in the assembly. Systems 1-6 were placed 5 mm away from microchannel and had a maximum energy product of 46 MGOe (N46 grade). Magnetic Systems 7-8 (not shown in Fig. 3) produced much higher magnetic field inside the microchannel and were comprised of single 0.75x 0.75 x 0.25 inch neodymium magnet placed very close to the microchannel wall. These systems were made of higher grade neodymium magnet with a maximum energy product of 52MGOe (N52 grade). Magnetic field strength was found to be maximum at the center of microchannel in the region of interest (ROI) and gradually diminishes near the inlet and outlet.

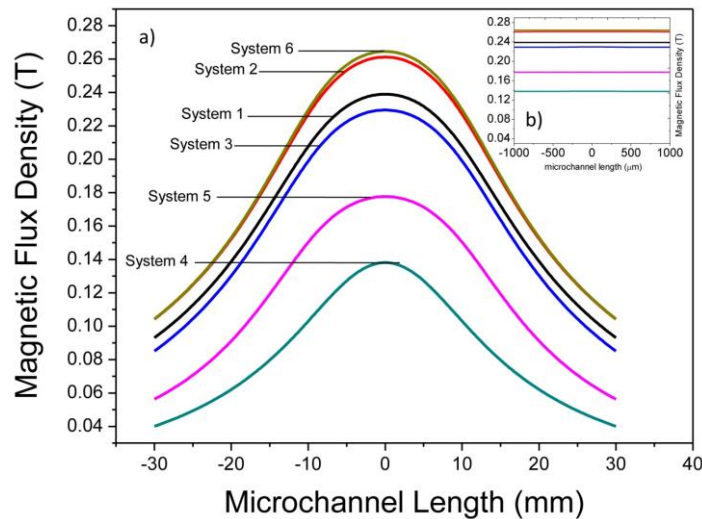


Fig. 3 Calculated Magnetic Flux density at center of microchannel along the length of the microchannel, and (b) shows the magnetic flux density in the region of interest (ROI) for different magnetic systems

## 4.2 Experimental results

In this work both a steady state and time-dependent operation of magnetic nanoparticle capturing process on a microfluidic platform were investigated. This simple setup employs an assembly of permanent magnets to attract nanoparticles in the microchannel continuously. The main design parameters of this multiphysics process are magnet field strength and gradient, magnetic nanoparticle size and properties; type of carrier fluid which translates to its viscosity and density, and most importantly microchannel dimensions. Based on the simple setup we have in this work, the operating parameters that were varied in this work are magnet field assembly which translates to magnetic field strength of the system, placement of permanent from microchannel and fluid flow rate. It is expected that these primary operating parameters can strongly influence the capturing process and were investigated. All experiments were conducted at room temperature and pressure with DI water and dilute magnetic nanoparticle concentrations.

### 4.2.1 Effect of magnetic system assembly on MNP capturing

In this section the effect of magnetic field assembly on the capturing process is investigated. Magnetic system were assembled based on different sizes and shape of permanent neodymium magnet (see Table 1) and were placed near the lower wall of microchannel as seen in Fig. 1. The magnetic field strength of these systems were calculated based on numerical simulation and have been discussed in detail in section 3.1. In these experiments System 1-6 were only compared based on the capturing efficiency of MNPs as they were kept 5 mm from the lower wall of the microchannel. A 50  $\mu\text{L}$  of MNPs solution with an initial concentration of 0.5 mg/mL was injected at the inlet of the microchannel at a flow rate of 0.3  $\mu\text{L}/\text{s}$ . The sample from the outlet is collected until all the solution has passed through the microchannel. It is taken in a cuvette and placed in Zetasizer to obtain unknown scattering intensity (kcps) of the sample. Previously determined calibration curve is used to convert the scattering intensity into unknown outlet concentration (mg/mL), which is used to compute the capturing efficiency of different magnetic system assemblies (System 1-6). Each experiment was performed in triplicates and average values together with standard deviation were reported. Figure 4 illustrate the effect of magnetic system assembly on the capturing of magnetic nanoparticles. It can be seen that system 2 and system 6 resulted in increased capturing of magnetic nanoparticles with capturing efficiency of 87% and 89.2% respectively, whereas system 4 was not successful in capturing enough magnetic nanoparticles (CE~ 36.7%) in the system. It can be seen that capturing process was not only dependent on the strength of magnetic field in the microchannel but also on the effective region in which the magnetic field was spread. For system 4 ( see Table 1) the effective width of the magnet assembly is only 0.375 inch and magnetic field intensity is 0.138 T, therefore it produced maximum magnetic force only in a small region and the magnetic field decreased dramatically within  $-10 \text{ mm} < x < 10 \text{ mm}$  ( see Fig. 3) from the magnet and reached a steady state. This resulted in less capturing of magnetic nanoparticles in the system. Moreover, effective width across x-axis for system 3 increased to 0.5 inch, which resulted in more capturing of MNPs as compared to system 4. For system 5 the effective width (~0.375 inch) was same as system 4 but due to addition of a square magnet of 0.75 x 0.75 inch at the bottom of assembly a slightly increase in capturing of MNPs was observed. It can also be seen from Figure 4b that capturing efficiency was also largely dependent on the magnetic flux density produced within the microchannel. A higher magnetic flux density over longer range will translate into higher magnetic force that can be obtained in the microchannel and will result in more capturing of magnetic nanoparticles. The gradient of

magnetic field also plays a critical role in increasing the magnetic force and can be optimized to further improve the performance. Based on this analysis system 2 was selected to be used for other parametric investigations as it produced higher magnetic field strength over longer range.

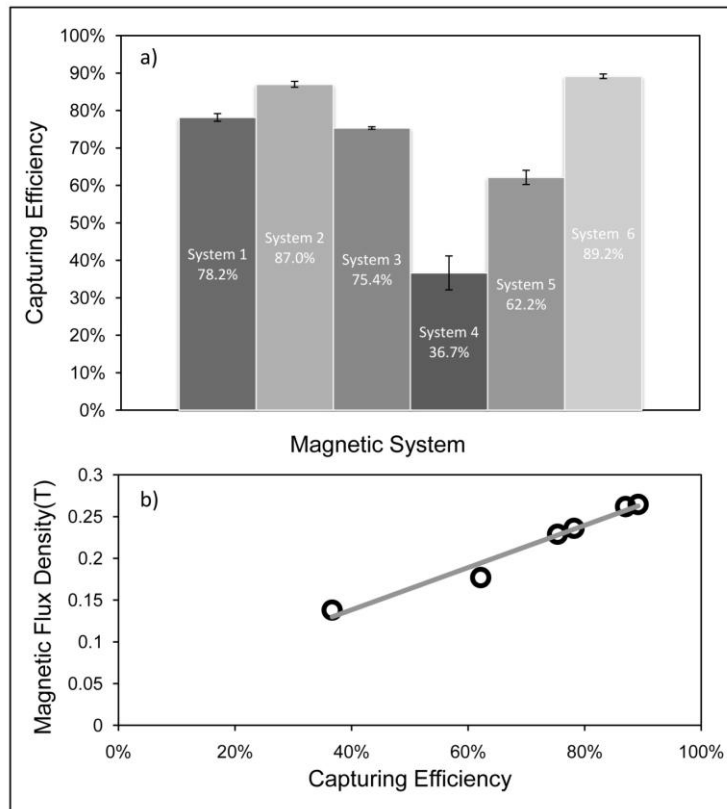


Fig. 4 Capturing Efficiency Analysis, (a) Comparison of capturing efficiency of different magnetic systems and (b) Magnetic Flux density versus capturing efficiency plot shows that magnetic systems producing high magnetic flux density in the microchannel have higher efficiency for trapping MNPs

#### 4.2.2 Effect of flow rates and placement of magnets on MNP capturing

In this section the effect of inlet flow rate and placement of magnetic field assembly (system 2) on the capturing process is investigated. Magnetic system 2 was initially placed at a distance of 0 mm from lower wall of microchannel and later displaced by a distance of 5, 10, 15, and 20 mm respectively. A 50  $\mu$ L of MNPs solution with an initial concentration of 0.5 mg/mL was injected at the inlet of the microchannel at different flow rates and outlet sample was collected and analyzed using Zetasizer instrument. Five different flow rate conditions were used for each position of magnetic system assembly. Capturing efficiency was computed using the concentration values obtained at the outlet. It can be seen from Fig. 5(a) that capturing efficiency increases with decrease in flow rates because decrease in flow rates will increase the residence time of magnetic

nanoparticles in the microchannel which will allow the nanoparticles to diffuse more, and experience larger magnetic force as compared to drag force. This will result in more magnetic nanoparticles being captured in the microchannel. It can also be seen from Fig. 5(a) that as we move the magnetic system away from microchannel, the effective magnetic force acting on the MNPs will decrease, which will lead to lesser capturing of magnetic nanoparticles. The effect of displacing the magnetic system away from the microchannel is more prominent at higher flow rates where magnetic nanoparticles follow the convection dominated regime and effective magnetic force acting on the magnetic nanoparticles is not enough to overcome drag force and cause capturing. Fig. 5(b) provides a general guideline based on these experiments for effectively increasing the capturing efficiency. It can be seen that a lower flow rates and magnetic system being more close to the microchannel is always desirable. In case that higher flow rates are needed to increase throughput, then choosing a system with higher magnet field strength in a longer range will be required.

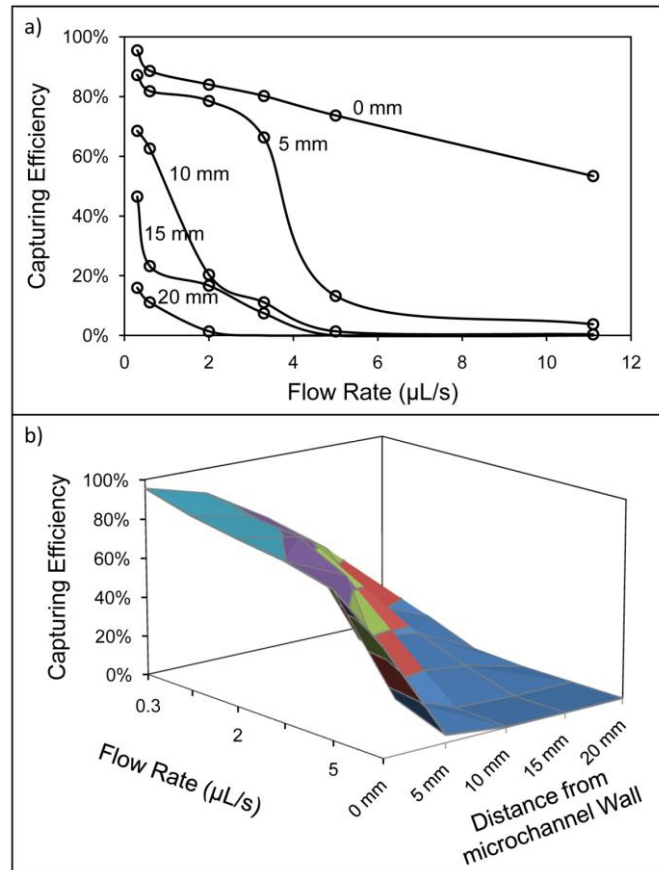


Fig. 5 (a) Variation of capturing efficiency of MNPs with flow rate of MNPs and distance of magnet from the lower wall of microchannel, and (b) 3D plot gives the guideline for obtaining higher capturing efficiency. A lower flow rate and magnet being closer to the microchannel is desirable

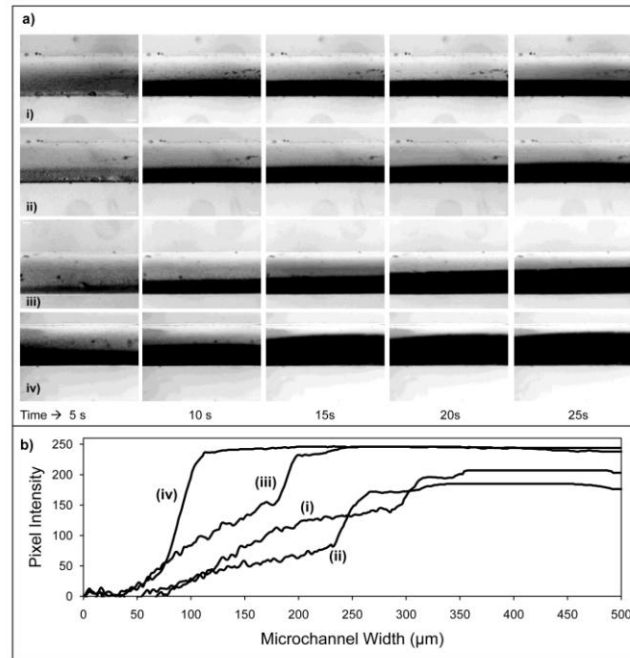


Fig. 6 (a) Micrograph of Magnetic Nanoparticle capturing experiments in the region of interest (ROI) at different times for four different magnetic systems, i) system 2, ii) system 6, iii) system 7, and iv) system 8. Magnetic systems were placed near the lower wall of the microchannel. Systems 2 & 6 were placed at 5 mm from the wall whereas Systems 7 & 8 was placed adjacent to the wall (0 mm), and (b) Pixel Intensity of the captured magnetic nanoparticles in ROI after 25s shows that system 8 has the highest amount magnetic nanoparticles captured in the microchannel

#### 4.2.3 Qualitative capturing analysis of MNPs

In this section qualitative analysis of the motion magnetic nanoparticles is performed with the aid of optical imaging using the digital microscope (Celestron 44340, Celestron Inc. USA). The translational stage of the microscope was used to place the microfluidic channel together with magnetic system assembly. Magnetic system 2 and 6, described earlier in the section were compared with magnetic system 7 and 8 (see Table 1.). The objective of camera acquired sequential images of the flowing magnetic nanoparticles at different times and transferred it to a computer for data acquisition. Image acquisition was performed using ImageJ software (NIH, USA) from the region of interest (ROI) under bright field lightning condition. Magnetic nanoparticle solution with a concentration of 0.5 mg/mL was injected from inlet at a flow rate of 0.3  $\mu\text{L/s}$ . It can be seen from figure 6a that magnetic nanoaprticles get captured near the magnetic system assembly on the lower wall of the microchannels. As the time progress more and more MNPs get captured. From the pixel intensity curve (see Figure 6b) magnetic system 7 and 8 shows higher percentage of MNPs capturing as compared to system 2 and 6. The reason for more trapping of MNPs was due to the fact that system 7 & 8 comprised of much higher grade Neodymium magnet (N52) which produced relatively higher magnetic field intensity inside the microchannel and they were placed closer to microchannel wall. Moreover, by placing Neodymium magnet (N52) with edge close to microchannel wall (system 8) a slightly higher

magnetic field strength together with more focusing of magnetic force was obtained. This eventually resulted in increased capturing of MNPs. From the analysis, it was found that system 8 produced the best results as overall it is easier to use higher grade Neodymium magnet and simple to assemble in the microfluidic setup when compared to system 2.

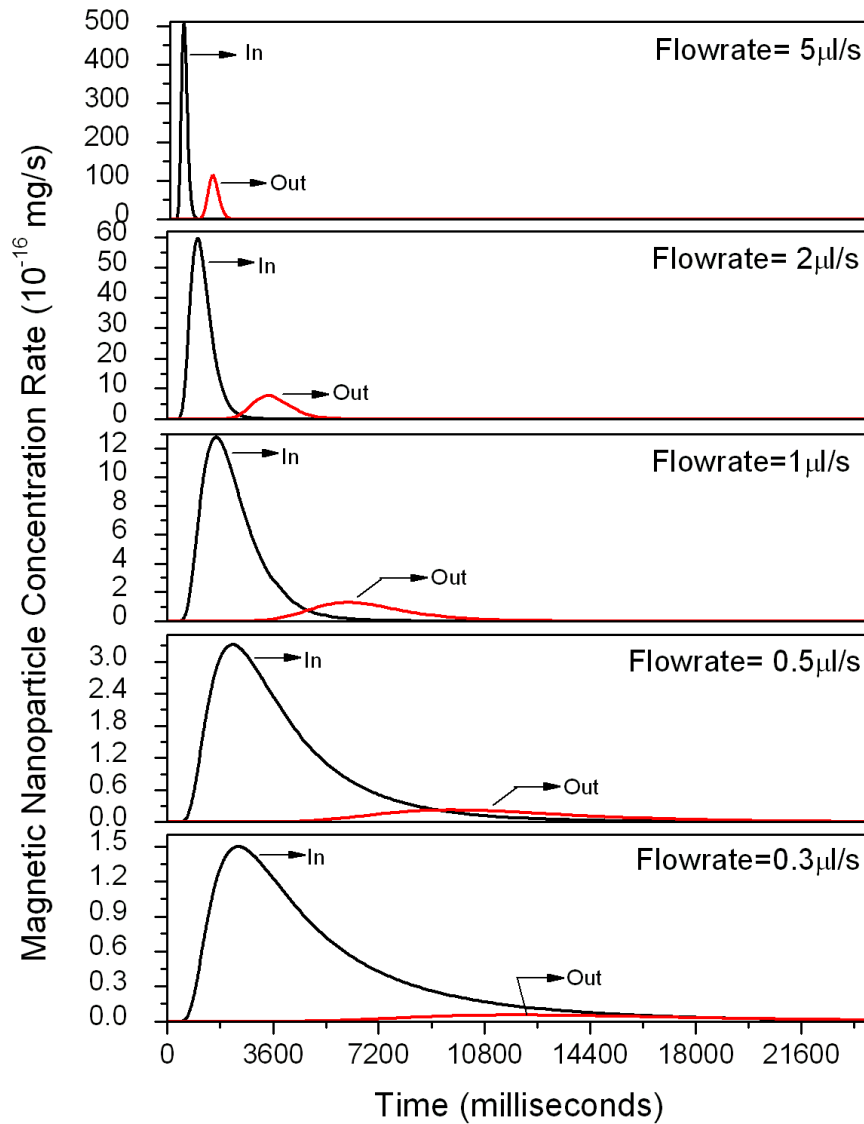


Fig. 7 Simulated magnetic nanoparticle concentration rate (mg/s) at the inlet and outlet of the microchannel for different flow rate conditions. Magnetic system 8 with MNPs concentration of 0.5 mg/ml was used in the simulation

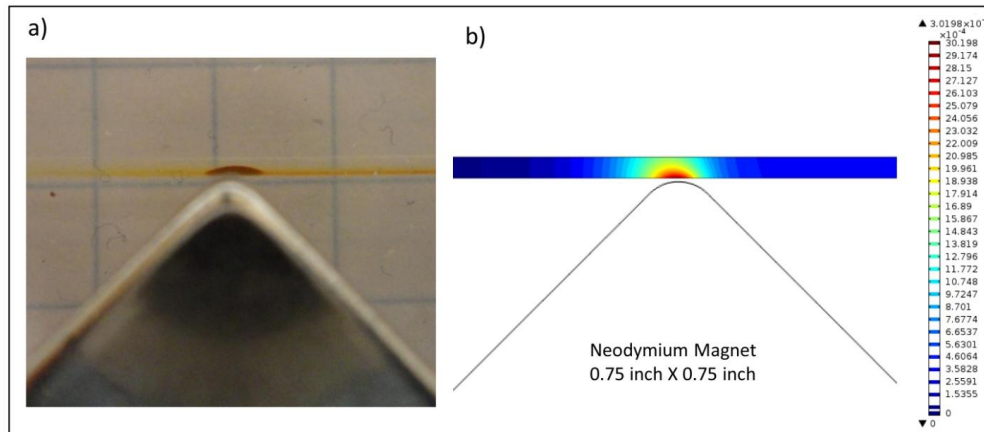


Fig. 8 Qualitative comparison of experiments and numerical simulation for capturing magnetic nanoparticle flowing at  $1 \mu\text{l/s}$  inside the microchannel using magnetic system 8. Initial concentration of  $0.5 \text{ mg/ml}$  was injected in the system from the right. The units of concentration is  $\text{mg/ml}$

#### 4.3 Numerical simulation and experimental validation

To predict the dynamics of magnetic nanoparticle capturing and understand the underlying physics affecting the process, a finite-element COMSOL-based mathematical model was developed as described in section 3. Numerical simulations were performed for magnetic microfluidic system 8 as shown in figure 1d.  $0.5 \text{ mg/ml}$  of magnetic nanoparticles were injected at the inlet under varying flow rate conditions. The results were compared and validated with experiments performed using similar magnetic system assembly. Fig. 7 shows the simulated magnetic nanoparticle concentration rate ( $\text{mg/s}$ ) at the inlet and outlet for different flow rate conditions. It can be seen that at lower flow rate ( $\sim 0.3 \mu\text{l/s}$ ) most of the nanoparticles gets trapped in the microchannel as a result only a small percentage exits the system. As the flow rate is increased more and more magnetic nanoparticles comes out of the microchannel. Similar observation was made in the experiments. At higher flow rates drag forces acting on the magnetic nanoparticles dominates when compared to magnetic forces as a result it is expected that more nanoparticles will leave the system and will not get trapped. In order to validate the numerical prediction, experiments were performed as described in section 4.2.1 using magnetic system 2 and 8 assembly for different flow rate conditions. A concentration  $0.5 \text{ mg/ml}$  of magnetic nanoparticles was injected into the microchannel and Zetasizer instrument was used to compute concentration exiting the system and finally the capturing efficiency. Magnetic system in both the scenarios was kept close to the microchannel ( $\sim 0 \text{ mm}$ ). Fig. 8 gives the qualitative comparison between experiments and numerical simulation for capturing of magnetic nanoparticle flowing at  $1 \mu\text{l/s}$  inside the microchannel. Magnetic system 8 was used in both experiments and numerical simulation. The results agree very well except for the fact that model did not account for the migration of magnetic nanoparticle along the lower wall of microchannel after they have been trapped. This obvious behavior could be due to particle-particle and particle-wall interaction, which makes some of magnetic nanoparticles leave the area of trapping and follow convective

flow along the microchannel wall. Both particle-particle and particle-wall interaction was considered negligible in the simulation. Also, the magnetic field in the region close to magnetic tip was not measured and could have played a critical role in trapping MNPs along the walls that result in concentration gradient in these regions. Overall, the model was successful in predicting the spot or region where majority of magnetic nanoparticles were captured in the microchannel. Fig. 9 gives the quantitative comparison of capturing efficiency of magnetic nanoparticles for both experiments and numerical simulation. It can be seen that numerical predictions were very close to experimental results. Slightly lower values were predicted by the mathematical model, this could be due to the incorrect magnetic force term in the model which did not take in account the surrounding medium that can very well influence magnetic field strength. Overall, the numerical prediction followed the same trend as the experimental results with capturing efficiency decreasing for higher flow rate conditions.

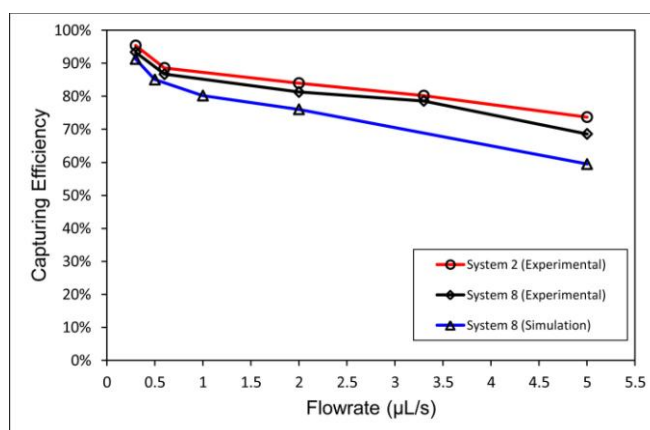


Fig. 9 Comparison of experimental and theoretical results for capturing of magnetic nanoparticles under varying flow rate conditions. Initial concentration of MNPs injected at the inlet was 0.5 mg/ml

#### 4.4 Numerical prototype & optimization

In this section the advantage of synchronizing numerical simulation with a simple low cost experimental proof-of-concept is highlighted. Numerical prototype and simulations can readily serve as “virtual experiments” and are used in this work to identify key design parameters and improve the functional performance of current magneto-fluidic capturing systems. It can be seen from previous experimental as well as theoretical results that the magnetic field strength, its orientation, effective range and magnetic field gradient are very important factors that influence the capturing of magnetic nanoparticles. Therefore, in order to enhance the performance magnetic field gradient was changed by placing a grooved iron bar on the opposite wall of the microchannel as seen in Fig. 10. The bar was 1mm wide and 4 mm long with 8 grooves of about 0.25 mm in diameter. In order to analyze the effect, virtual simulation were done and compared with base system comprising only of magnetic system 8 assembly. From Fig. 10, we can see that by placing the groove structure the magnetic flux density increased from 0.85 to 1.05 Tesla (see Fig. 10(a) (ii) and 10(b) (ii)) at the center of microchannel. It can also be seen the magnetic field was more focused in the region of interest where magnetic nanoparticle are expected to be trapped and

higher gradient of magnetic field was achieved. Fig. 11 illustrate the effect of placing grooved iron bar on the inlet and outlet concentration rate of magnetic nanoparticles computed using the mathematical model. Initially, 0.5 mg/ml of MNPs were injected into the system at a flow rate of 1  $\mu\text{l/s}$ . It can be seen that more magnetic nanoparticles gets trapped (see Fig. 11(b)) when grooved iron bar is placed in the vicinity of microchannel since the outlet concentration rate was decreased when compared to system without grooved structure. This proves that presence of grooved iron, close to the microchannel is able to induce a large magnetic field gradient which translates into an enhanced magnetic force on the magnetic nanoparticles. Capturing efficiency was computed as described in previous section and it was found that there was 12% increase in trapping magnetic nanoparticles flowing at 1  $\mu\text{l/s}$  when grooved-iron bar was placed in vicinity. This strategy is very useful in enhancing the performance of magnetic microfluidic system in scenarios where higher flow rates conditions are required. Despite the successful demonstration of incorporating iron structure in the setup for magnetic nanoparticle capturing process, one should note that the current system can further be optimized in a number of ways. Other improvements which can be done to further enhance the device performance are parameters such as the dimension of the main channel as well as the flow rates for the carrier fluid, magnetic system assembly. These parameters are critical in dictating the resulting capturing efficiency and can very well be optimized using mathematical tool before implementing in the fabrication process and device development. Overall, the numerical simulation was helpful in testing one of the hypotheses without actually performing the experiments and identifying the key design parameters that will be very useful in enhancing the functional performance of magneto-fluidic capturing systems.

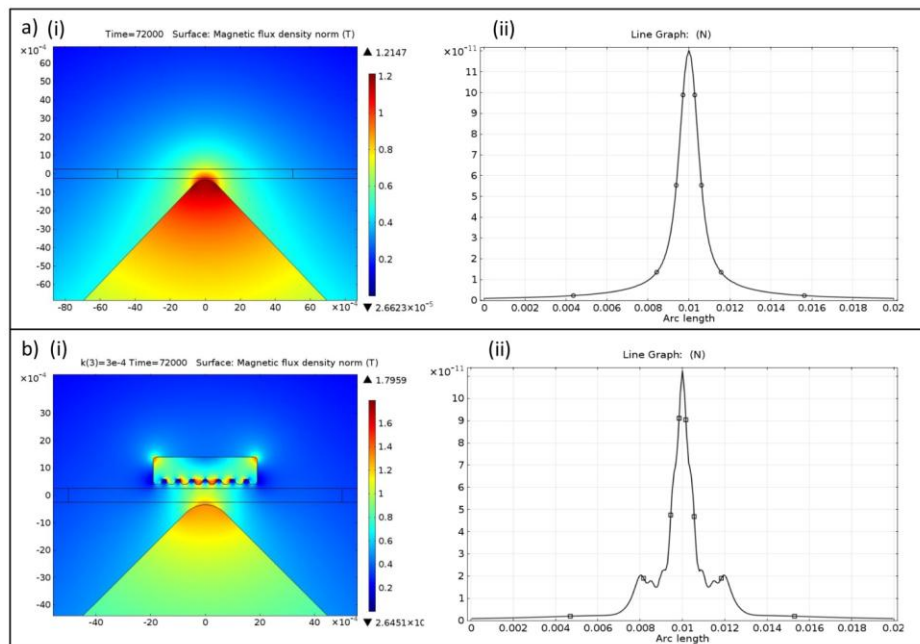


Fig. 10 Simulated magnetic field intensity in Tesla (a) Magnetic System 8 (i) 2D surface plot of Magnetic field Intensity, (ii) Magnetic force along the x-axis in the center of microchannel( $y=0$ ) and (b) System 8 with iron grooved bar (i) 2D surface plot of Magnetic field Intensity, (ii) Magnetic force along the x-axis in the center of microchannel( $y=0$ )

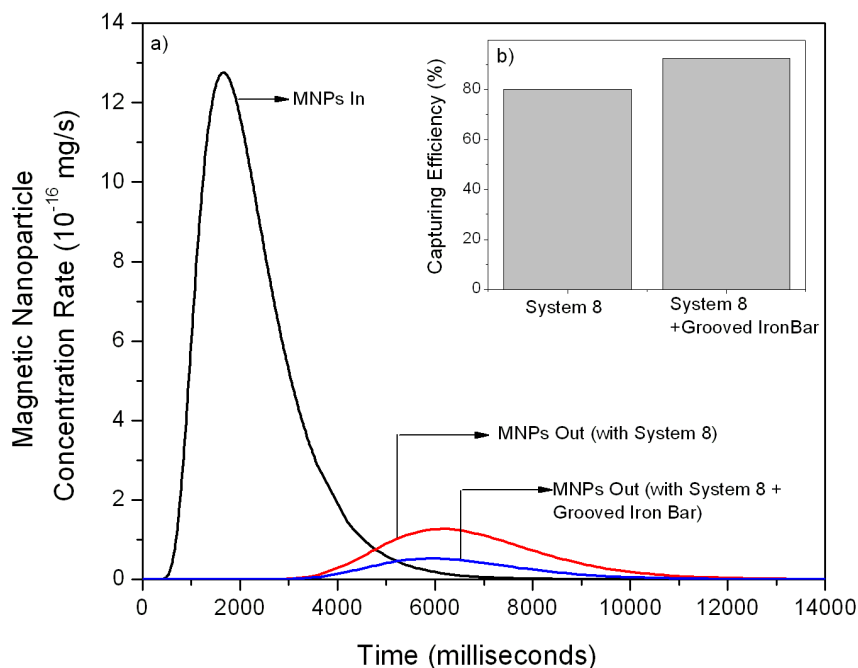


Fig. 11 (a) Simulated magnetic nanoparticle concentration rate (mg/s) at the inlet and outlet of the microchannel for Magnetic system 8 with and without grooved-iron bar in the vicinity of microchannel. MNPs concentration of 0.5 mg/ml was used in the simulation and (b) Capturing efficiency computed based on incoming and outgoing mass of magnetic nanoparticles for both the system

## 5. Conclusions

In this work, a simple, low cost and generic microfluidic platform is developed to study the dynamics of magnetic nanoparticle capturing process in microfluidic channel. Compared to the conventional MEMS fabrication technology, microfluidic channels were fabricated using a novel micromolding method that can be done without a clean room and at much lower cost and time. Proof-of-concept experiments were combined with finite element simulation based on drift-diffusion model to enhance the performance of the magnetic microfluidic system. Parametric investigations using both experiments and theoretical predictions were performed. It was found that flow rate and magnetic parameters influence the transport magnetic nanoparticles in the microchannel and control the capturing efficiency. Mathematical model was validated using the experimental results and was further used to enhance the performance of the capturing process by introducing an iron-grooved bar in the virtual simulations. Overall, this work demonstrated that a simple low cost experimental proof-of-concept setup can be synchronized with advanced numerical simulation to design and improve the functional performance of magneto-fluidic bioseparation systems.

## Acknowledgements

The author greatly acknowledge the support from National Science Foundation (CMMI-1030289). This work was partly supported by the National Natural Science Foundation of China (No. 31101274)

## References

- Ahn, C.H., Allen, M.G., Trimmer, W., Jun, Y.N. and Erramilli, S. (1996), "A fully integrated micromachined magnetic particle separator", *J. Microelectromech. S.*, **5**, 151-158.
- Berry, C.C. and Curtis, A.S.G. (2003), "Functionalisation of magnetic nanoparticles for applications in biomedicine", *J. Phys. D Appl. Phys.*, **36**, R198-R206.
- Brauer, J.R. (2007), "Finite-element computation of magnetic force densities on permeable particles in magnetic separators", *IEEE T. Magn.*, **43**, 3483-3487.
- Bu, M.Q., Christensen, T.B., Smistrup, K., Wolff, A. and Hansen, M.F. (2008), "Characterization of a microfluidic magnetic bead separator for high-throughput applications", *Sensor. Actuat. A-Phys.*, **145-146**, 430-436.
- Choi, J.W., Oh, K.W., Thomas, J.H., Heineman, W.R., Halsall, H.B., Nevin, J.H., Helmicki, A.J., Henderson, H.T. and Ahna, C.H. (2002), "An integrated microfluidic biochemical detection system for protein analysis with magnetic bead-based sampling capabilities", *Lab Chip.*, **2**, 27-30.
- Clime, L., Boris, L.D. and Teodor, V. (2007), "Dynamics of superparamagnetic and ferromagnetic nano-objects in continuous-flow microfluidic devices", *IEEE T. Magn.*, 2929-2931.
- Deng, T., Prentiss, M. and Whitesides, G.M. (2002), "Fabrication of magnetic microfiltration systems using soft lithography", *Appl. Phys. Lett.*, **80**(3), 461-463.
- Furlani, E.P. (2001), *Permanent magnet and electromechanical devices : materials, analysis and applications*, New York: Academic Press Inc.
- Furlani, E. P. (2006), "Analysis of particle transport in a magnetophoretic microsystem", *J. Appl. Phys.*, **99**.
- Furlani, E.P. and Ng, K.C. (2006), "Analytical model of magnetic nanoparticle transport and capture in the microvasculature", *Phys. Rev. E.*, **73**.
- Furlani, E.P. (2010), "Magnetic biotransport: analysis and applications", *Material*, **3**, 2412-2446.
- Gerber, R., Takayasu, M. and Friedlander, F.J. (1983), "Generalization of HGMS theory: the capture of ultrafine particles", *IEEE T. Magn.* **319**, 2115-2117.
- Gijs, M.A.M. (2004), "Magnetic bead handling on-chip: new opportunities for analytical applications", *Microfluid. Nanofluid.*, **1**, 22-40.
- Hahn, Y.K., Jin, Z.W., Kang, J.H., Oh, E.K., Han, M.K., Kim, H.S., Jang, J.T., Lee, J.H., Cheon, J.W., Kim, S.H. Park, H.S. and Park, J.K. (2007), "Magnetophoretic immunoassay of allergen-specific IgE in an enhanced magnetic field gradient", *Anal. Chem.*, **79**(6), 2214-2220.
- Hayes, M.A., Polson, M.A., Phayre, A.N. and Garcia, A.A. (2001), "Flow-based microimmunoassay", *Anal. Chem.*, **73**(24), 5896-5902.
- Kim, M.C., Kim, D.K., Lee, S.H., Amin, M.S., Park, I.H., Kim, C.J. Zahn, M. (2006), "Dynamic characteristics of superparamagnetic iron oxide nanoparticles in a viscous fluid under an external magnetic field", *IEEE T. Magn.*, **42**(4), 979-982.
- Lee, C.S., Lee, H. and Westervelt, R.M. (2001), "Microelectromagnets for the control of magnetic nanoparticles", *Appl. Phys. Lett.*, **79**(20), 3308.
- Lehmann, U., Vandevyver, C., Parashar, V.K. and Gijs, M.A.M. (2006), "Droplet-based DNA purification in a magnetic lab-on-a-chip", *Angewandte Chemie-Int. Ed.*, **45**(19), 3062-3067.
- Manz, A., Graber, N. and Widmer, H.M. (1990), "Miniaturized total chemical-analysis systems – a novel concept for chemical sensing", *Sensor. Actuat. B Chem.*, **1**(1-6), 244-248.

- McCloskey, K.E., Chalmers, J.J. and Zborowski, M. (2000), "Magnetophoretic mobilities correlate to antibody binding capacities", *Cytometry*, **40**, 307-315.
- Pamme, N. (2006), "Magnetism and microfluidics", *Lab Chip.*, **6**, 24-38.
- Pankhurst, Q.A., Connolly, J., Jones, S.K. and Dobson, J. (2003), "Applications of magnetic nanoparticles in biomedicine", *J. Phys. D Appl. Phys.*, **36**(13), R167-R181.
- Rida, A. and Gijss, M.A.M. (2004), "Dynamics of magnetically retained supraparticle structures in a liquid flow", *Appl. Phys. Lett.*, **85**, 4986.
- Rosensweig, R. (1997), *Ferrohydrodynamics*. New York: Dover Publication Inc.
- Shih, P.H., Shiu, J.Y., Lin, P.C., Lin, C.C., Veres, T. and Chen, P. (2008), "On chip sorting of bacterial cells using sugar-encapsulated magnetic nanoparticles", *J. Appl. Phys.*, **103**(7).
- Smistrup, K., Kjeldsen, B.G., Reimers, J.L., Dufva, M., Petersena, J. and Hansena, M.F. (2005), "On-chip magnetic bead microarray using hydrodynamic focusing in a passive magnetic separator", *Lab Chip.*, **5**, 1315.
- Smistrup, K., Torsten, L.O., Hansen, M.F. and Tang, P.T. (2006), "Microfluidic magnetic separator using an array of soft magnetic elements", *J. Appl. Phys.*, **99**(8), 08P102 - 08P102-3.
- Sullivan, S.P., Akpa, B.S., Matthews, S.M., Fisher, A.C., Gladden, L.F. and Johns, M.L. (2007), "Simulation of miscible diffusive mixing in microchannels", *Sensor. Actuat. B Chem.*, **123**, 1142-1152.
- Suzuki, H., Ho, C.M. and Kasagi, N. (2004), "A chaotic mixer for magnetic bead-based micro cell sorter", *J. Microelectromech. S.*, **13**(5), 779-790.
- Yellen, B.B. and Friedman, G. (2004), "Programmable assembly of colloidal particles using magnetic micro-well templates", *Langmuir*, **20**, 2553.
- Xia, N., Hunt, T.P., Mayers, B.T., Alsberg, E., Whitesides, G.M., Westervelt, R.M., Ingber, D.E. (2006), "Combined microfluidic-micromagnetic separation of living cells in continuous flow", *Biomed. Microdevices*, **8**(4), 299-308..